

# The plan for a super $\eta$ factory at Huizhou accelerator complex

Xurong Chen<sup>1,2</sup>, Xionghong He<sup>1,2</sup>, Qiang Hu<sup>1,2</sup>, Dexu Lin<sup>1,2</sup>, Yang Liu<sup>1,2</sup>, Hao Qiu<sup>1,2</sup>, Xu Sun<sup>1,2</sup>, Ye Tian<sup>1,2</sup>, Rong Wang<sup>1,2</sup>, Honglin Zhang<sup>1,2</sup>, Yapeng Zhang<sup>1,2</sup>, and Chengxin Zhao<sup>1,2</sup>

<sup>1</sup>Institute of Modern Physics, Chinese Academy of Sciences, Lanzhou 730000, China

<sup>2</sup>School of Nuclear Science and Technology, University of Chinese Academy of Sciences, Beijing 100049, China

May 2024

## Abstract

As an approximate Goldstone boson with zero quantum number and zero standard model charge, the decay processes of long-lived  $\eta$  meson offer a unique opportunity to explore new physics beyond the standard model and new sources of CP violation, as well as test the low-energy QCD theory and measure the fundamental parameters of light quarks. To pursue these goals in the physics frontiers, we propose a plan to construct a super  $\eta$  factory at HIAF high-energy terminal or at CiADS after its energy upgrade. The high-intensity proton beam at HIAF enables the production of a vast number of  $\eta$  samples, exceeding  $10^{13}$  events per year in the first stage, utilizing multiple layers of thin targets made of light nucleus. This paper presents the physics goals, the first-version conceptual design of the spectrometer, and some preliminary simulation results.

## 1 Introduction

The high-luminosity frontier is one way to the new physics [1], as any small deviations from the standard model (SM) predictions in the high-precision measurements are implications of the new physics beyond the SM. In the next decade, the upcoming high-intensity proton accelerator will offer a unique opportunity for searching the new physics at an unprecedented level. Actually, there are more and more signs of new physics, such as the anomalous muon magnetic moment  $(g - 2)_\mu$  [2–4], the X17 boson from the decay of the excited state of  $^8\text{Be}$  [5–7], the lepton flavor universality violation in bottom quark decays [8–12], the excesses of the cosmic positron and electron [13–16], the narrow  $\gamma$  ray emission from the galactic bulge [17], and the unexplored natures of dark matter [18–22] and dark energy [23–27]. Up to now, physicists do not observe any new physics in the high-energy frontier with the large hadron collider. Therefore, some people argue that the new physics of the hidden sector is at low energies [28, 29], but it is faintly coupled to SM matter, which makes it elusive. For example, the production rates of the light portal particles connecting the hidden sector with the SM sector are magnitudes higher at low energies [28]. Moreover, for the low-energy fixed target experiment, the luminosity can be much higher with a thick target.

The  $\eta$  meson is of particular interests, as it is an approximate Goldstone boson from spontaneous chiral symmetry breaking and with zero SM charge [30]. Many strong and electromagnetic decay channels of  $\eta$  are forbidden at the leading order, which relatively enhance the rare decay channels of  $\eta$  meson that are sensitive to new physics. The  $\eta$  meson is a wonderful low-energy lab for searching the new physics beyond the SM, via observing the dark portal particles from  $\eta$  decays [28, 29, 31] or measuring the small discrete symmetry breaking such as CP violation and charged lepton flavor violation [32, 33]. A thorough discussion on the theoretical developments of  $\eta$  and  $\eta'$  decays were impressively given in a recent review article [32], regarding the high-precision tests of fundamental physics. There are four kinds of portals predicted by the latest theoretical models: the vector portal [34–37], the scalar portal [38–44], the axion-like portal [45–49] and the heavy neutral lepton portal [50–52]. The portal particles are important in theories for connecting the Dark Sector and the SM Sector. All these light portal particles can be accessed from the rare decays of  $\eta$  meson [31, 32]. The symmetry and symmetry breaking are at the heart of modern physics. Finding new sources of CP violation is essential to explain the baryon-antibaryon asymmetry in the world where we live in. Any charged lepton

flavor violation is a strong indication of beyond SM physics. Many  $\eta$  decay channels provide the precise tests of these symmetry breakings. The precise measurements of  $\eta$  decay channels are critical for us to understand the C, P, T, CP, and charged lepton flavor violations.

In addition to the new physics searches, the high-precision study of  $\eta$  decay provides a unique way to test the quantum chromodynamics (QCD) theory at low energies [53–58], to probe the  $\eta$  structure [59–65], to precisely measure the mass difference of light quarks [66–71], to verify the axial anomaly [72–74]. From the electromagnetic decay channels associated with virtual and real photons, the  $\eta$  transition form factor can be constrained with much smaller uncertainties [59–64], which eventually helps us better understanding the muon anomalous magnetic moment [2–4]. The quark masses are the fundamental parameters of the SM. Measuring the isospin-breaking  $3\pi$  decay channels of  $\eta$  is one important way to experimentally constrain the light quark masses. The high-precision measurements at a super  $\eta$  factory will reduce the uncertainties of QCD parameters significantly. The precise measurements of some  $\eta$  rare decays provide a strict test of chiral perturbation theory at high orders [75], which is a rigorous and effective theory for the strong interaction at low energies.

As the  $\eta$  meson decays involve such plentiful physics, there are already many measurements of  $\eta$  decays with the current facilities worldwide. First, there are the hadronic productions of  $\eta$  from fixed-target experiments, such as the WASA-at-COSY experiment [76–78] and the LHCb experiment [79, 80]. The WASA-at-COSY collaboration used the proton beam at COSY and an internal pellet target, and the statistic of  $\eta$  events is at the level of  $10^8$ . Second, the radiative decays of  $\phi$  and  $J/\psi$  at electron-positron colliders produced a decent amount of  $\eta$  samples of low background. The number of  $\eta$  events from  $\phi$  decay by KLOE collaboration is at the level of  $10^8$  [81–84], while the number from  $J/\psi$  decay by BESIII collaboration is at the level of  $10^7$  [85–89]. Third, the photoproduction experiment is also a clean way to produce  $\eta$  meson, such as the A2 experiment at MAMI [59, 90, 91], and the JLab Eta Factory (JEF) [32, 92] by exploiting the Primakoff effect [93]. JLab has a long tradition of studying the neutral meson physics via the Primakoff reaction [94, 95]. For JEF experiment, around  $10^9$  tagged  $\eta$  events will be collected in years, with the GlueX spectrometer [96, 97]. Thanks to the high-performance calorimeter and the high energy of the incident photon up to 11 GeV, the backgrounds are well in control for the neutral decay channels. The JEF experiment has the advantages in measuring the neutral decay channels of  $\eta$  meson.

Aiming at the intriguing discovery potentials of light dark portal particles and the strong tests of the standard model, it is imperative to build a super  $\eta$  factory with the high-intensity accelerators, to acquire the unprecedented  $\eta$  meson samples. To pursue a vast number of  $\eta$  events, REDTOP (Rare Eta Decays To Observe Physics beyond the standard model) experiment [31] is proposed for the 2021 US community study on the future of particle physics, with some novel detector techniques. In China, a High-Intensity heavy-ion Accelerator Facility (HIAF) is under construction at Huizhou city, by Institute of Modern Physics (IMP), Chinese Academy of Sciences (CAS), which is competitive in the beam intensity. With this near-future infrastructure, we suggest a super  $\eta$  factory at HIAF high-energy terminal. There is no doubt that the proposed Huizhou  $\eta$  factory will bring many fruitful physics results and it will push the accelerator and detector technologies to a much higher level.

The organization of paper is as follows. The suggested Huizhou  $\eta$  factory and its physics goals are introduced in Sec. 2. The conceptual design of the spectrometer is present in Sec. 3. Some preliminary results of the simulations are shown in Sec. 4, for some golden channels of the experiment. In Sec. 5, a concise summary and the outlooks are given.

## 2 Huizhou $\eta$ factory and its goals

The HIAF is an under-construction major national science infrastructure facility of China, located in Huizhou city, Guangdong province in Southern China [98–100]. The construction of HIAF started from December of 2018, and it is going to be ready for commissioning at the end of 2025. The HIAF is an accelerator complex mainly consisting of a superconducting electron-cyclotron-resonance ion source, a continuous-wave superconducting ion linac, a booster synchrotron, a high-energy fragment separator, and a high-precision spectrometer ring. The layout of HIAF is depicted in Fig. 1. Many terminals are designed along the accelerator complex for experiments and applications. With the high-intensity technology, HIAF is not only a powerful infrastructure for the frontier studies in nuclear physics, high energy density physics, and atomic physics, but also an excellent platform for heavy-ion applications in life, material and space sciences [100]. HIAF is featured with delivering the unprecedented intense ion beams from hydrogen to uranium with energy up to GeV/u.

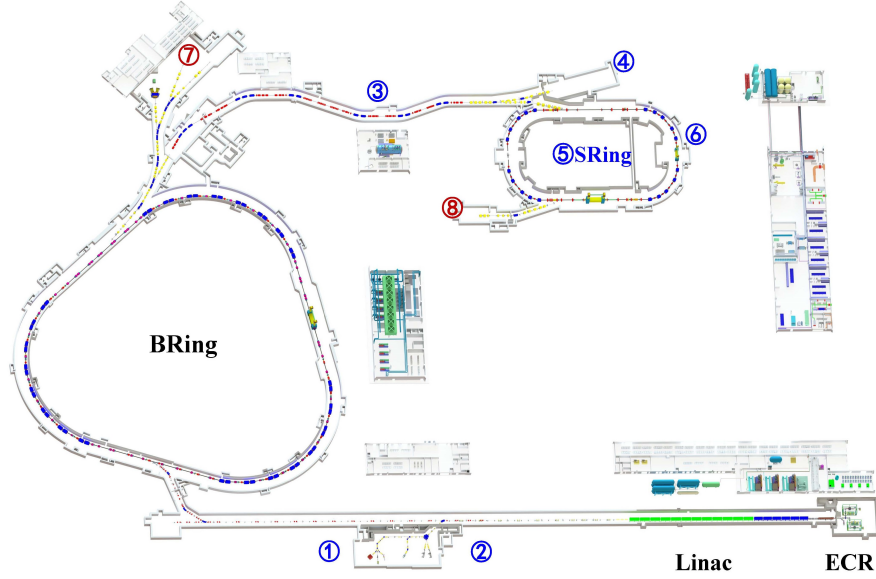


Figure 1: The layout of HIAF facility. The number “⑦” indicates where the high-energy multidisciplinary terminal locates.

The maximum energy for the proton beam is 9.3 GeV [98–100]. With the heavy-ion beam, HIAF provides an extraordinary platform for the studies of hypernuclei and the phase structure of high-density nuclear matter; With the high-energy proton beam, HIAF gives an excellent opportunity for studying light hadron physics and building a  $\eta$  factory.

At HIAF, the intensity of the proton beam is higher than  $10^{13}$  ppp (particles per pulse), and the kinematic energy of the proton can reach 9 GeV through the accelerations of the ion linac and the booster ring [98–100]. The pulse rate is around several Hz. A super  $\eta$  factory is suggested to be build at the high-energy multidisciplinary terminal after the booster ring, the terminal “⑦” shown in Fig. 1. The target is made of multiple foils of light nucleus ( ${}^7\text{Li}$  or  ${}^9\text{Be}$ ) with 1 cm gaps, which significantly reduces the coincident background from the same vertex with no decline of the luminosity at the same time. With the proton beam and light nuclear target, the  $\eta$  meson is produced efficiently with controlled background at HIAF. The beam-energy thresholds are 1.26 GeV and 2.41 GeV for  $\eta$  and  $\eta'$  productions respectively. In the proton-proton scattering and at beam energy of 1.8 GeV, the cross section of  $\eta$  meson production is large [101–104], judged by the previous COSY data (around  $100\ \mu\text{b}$ ) [101]. For the nuclear target, the cross section for  $\eta$  meson production is even higher. Based on the HIAF beam intensity and a lithium target of 1 cm thickness in total, the luminosity is above  $10^{35}\ \text{cm}^{-2}\text{s}^{-1}$  for the Huizhou eta factory experiment. Regardless of the capabilities of the detector and data acquisition systems, the  $\eta$  production rate can be higher than  $10^8\ \text{s}^{-1}$  on a light nuclear target ( $> 10^{15}$  per year).

China initiative Accelerator Driven Sub-critical system (CiADS) is another high-intensity proton accelerator designed for the verification of the principle of nuclear waste disposal [105–110]. It provides a much powerful continuous proton beam. The designed full power of CiADS accelerator is 2.5 MW, with the beam intensity of  $3.15 \times 10^{16}$  pps. The CiADS is also a good choice for building a super  $\eta$  factory, so long as the energy of CiADS is upgraded to about 2 GeV. Since the upgrade of CiADS accelerator is anticipated to take many years, the proposed Huizhou  $\eta$  factory will be located mainly at HIAF high-energy terminal.

At Huizhou  $\eta$  factory, there is going to be a huge statistic of  $\eta$  meson samples, about four magnitudes more than the current  $\eta$  events achieved worldwide. With such an enormous yield of  $\eta$  mesons, the main physical goals of Huizhou  $\eta$  factory are to discover the new physics via the search for new particles and the discrete symmetry breaking, and to study the SM with a very high precision. The new particles of interests from  $\eta$  and  $\eta'$  decays are the predicted light portal particles below GeV which connect faintly the SM sector with the Hidden sector, such as the dark vector particles [34–37], the dark scalar particles [38–44], and the axion-like particles [45–49]. The protophobic X17 boson of the fifth force [5–7] also can be studied via rare  $\eta$  decay. The huge amount of  $\eta$  mesons provides us a good opportunity to study new sources of CP violation,

Table 1: The list of the main physics goals of Huizhou eta factory.

Physics goals		Decay channel
New physics	Dark photon & X17	$e^+e^-\gamma$
	Dark higgs	$\pi^+\pi^-\pi^0$ $\pi^0e^+e^-$
	Axion-like particle	$\pi^+\pi^-e^+e^-$ $\pi^+\pi^-\gamma\gamma$
	CP violation	$\pi^+\pi^-\pi^0$ $\pi^+\pi^-e^+e^-$
	Lepton flavor violation	$\gamma\mu^+e^-$ / c.c. $\mu^+e^-$ / c.c.
Precision test of the SM	$\eta$ transition form factor	$e^+e^-\gamma$ $e^+e^-e^+e^-$ $\pi^+\pi^-\gamma$
	Light quark masses	$\pi^+\pi^-\pi^0$ $\pi^0\pi^0\pi^0$
	Chiral anomaly	$\gamma\gamma$ $\pi^+\pi^-\gamma$
	Beyond SM weak decay	$e^+e^-$
	Test chiral perturbation theory	$\pi^+\pi^-\gamma\gamma$ $\pi^0\gamma\gamma$

which is essential for the matter-antimatter asymmetry in the universe, and to search for the charged lepton flavor violation, which is a clear and strong sign of new physics. Last but not least, the precise measurements of  $\eta$  decays are critical for high precision study of the standard model, such as strictly constraining the light quark mass difference, precise measurement of meson structure, and high-precision test of chiral perturbation theory. The main physics interests are listed in Table 1. Since the spectrometer of Huizhou eta factory excels particularly in measuring the charged particles, the charged decay channels are the golden channels of high priority for the proposed experiment, such as  $\eta \rightarrow \pi^+\pi^-\pi^0$ ,  $\eta \rightarrow e^+e^-\gamma$ ,  $\eta \rightarrow \pi^+\pi^-e^+e^-$ , and  $\eta \rightarrow e^+e^-$ .

### 3 A compact and large-acceptance spectrometer with silicon pixels

With the fast development of the monolithic silicon pixel technology [111], we came up with an idea of large acceptance and compact spectrometer with silicon pixels to detect the final-state particles at a high event rate. The current design of the spectrometer include four main parts: the tracking system for charged particles made of silicon pixels, the time of flight detector for particle identification made of silicon Low-Gain Avalanche Detector (LGAD), the Electro-Magnetic calorimeter (EM calorimeter) for photon measurement made of lead glass [112], and a super-conducting solenoid. The 3D design of the spectrometer is shown in Fig. 2. Thanks to the high granularity and small position resolution of the silicon pixel detector, it is a quite compact spectrometer with a small volume. Therefore the EM calorimeter and the solenoid are of small size, which reduce the cost for fabricating the spectrometer. The inner radius of the super-conducting solenoid is just about 70 centimeters and all the main detectors are inside the solenoid.

The multi-layer target is put inside the spectrometer close to the entrance, so that to have a large acceptance for the fixed-target experiment. With the current conceptual design of spectrometer, all forward particles

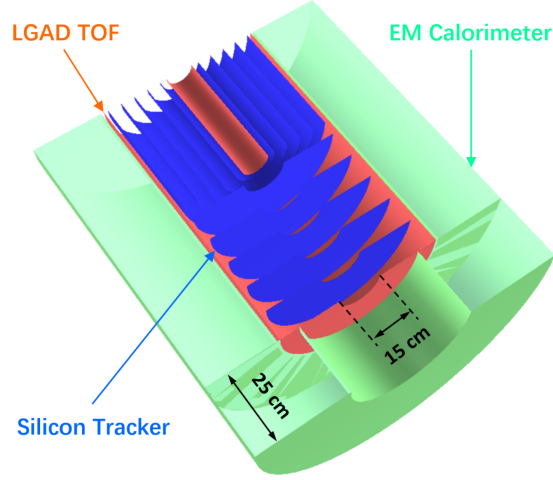


Figure 2: The conceptual design of a compact spectrometer for  $\eta$  factory. The spectrometer mainly relies on the silicon detector technology, with the monolithic silicon pixel tracker and the fast LGAD TOF detector of low material budget. The silicon tracker is wrapped with a fast lead-glass calorimeter for high-energy photons.

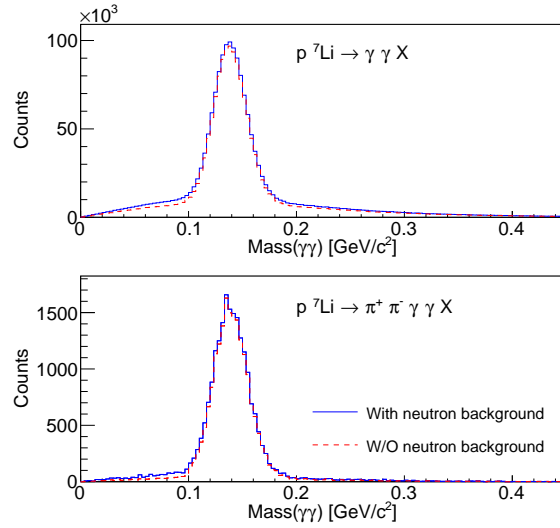


Figure 3: The invariant mass distributions of two  $\gamma$ 's from the simulations with and without the neutron contamination. The  $p\text{-}^7\text{Li}$  events are generated with GiBUU package. The  $\gamma$ 's are detected under two different situations: (1) we assume that the calorimeter can NOT distinguish the neutron from the photon (with neutron background); (2) we assume that the calorimeter can well distinguish the neutron from the photon (without neutron background).

except the small-angle particles are covered without dead zones.

To achieve a high-rate capacity of the silicon pixel tracker, the silicon detector group has tried the dual measurements of the energy and the arrival time of each pixel [113–117]. With the different arrival times, the hits from different events can be distinguished. For the first-version of the silicon pixel chip ( $\sim 1 \times 1 \text{ cm}^2$ ) of about 100k pixels, it takes about  $600 \mu\text{s}$  to read all the pixels in the scan mode, and the resolution of arrival time is about 400 ns. The objectives of the future silicon pixel chip are the resolution of 10 ns for the arrival time, the pixel size of  $30 \mu\text{m}$ , and the scan time of  $100 \mu\text{s}$  for about 100k pixels. Under the particle multiplicity of Huizhou eta factory and with the pixel chip more than 5 cm away from the interaction point, the designed silicon pixel chip can easily record the events at the event rate of more than 100 MHz.

For the current conceptual design of the spectrometer, the material for the calorimeter is lead glass which generates only the prompt Cherenkov photons. Therefore it has a good time resolution around 100 ps for the particle detection. At the same time, the lead glass is not sensitive to the hadronic shower initiated by nucleons and pions, which means it has a small efficiency for neutron background and offers additional hadron background suppression capability. Our Geant4 simulation [118–120] finds that the low-energy neutrons ( $E_k < 0.3 \text{ GeV}$ ) generate almost no hit in the lead glass calorimeter, and the high-energy neutron ( $E_k > 1 \text{ GeV}$ ) has just about 45% probability to deposit more than 10 MeV energy in the calorimeter. As most of the neutrons from  $pA \rightarrow X$  collision are low energy neutrons, the neutron background in the photon measurement can be eliminated effectively with the lead glass calorimeter. With the inelastic events generated with GiBUU package [121–124], we show in Fig. 3 the invariant mass distributions of two photons, with and without the neutron background. The background for the  $\pi^0$  signal due to the neutron contamination is negligible, especially for the channel  $p^7\text{Li} \rightarrow \pi^+\pi^-\pi^0 X$ . In the simulation, the threshold for a hit in the calorimeter corresponds to the signal generated by a 50 MeV photon. The neutron deposits less energy in the calorimeter comparing to the photon, and with the same amount of energy deposition, the hadronic shower initiated by the neutron generates less Cherenkov photons. That is why the abundant neutron background at low energy is strongly suppressed in the measurement of photon and  $\pi^0$ .

Although lead glass calorimeter is effective at suppressing hadron backgrounds and is cost-effective, it has significant drawbacks compared to conventional crystal calorimeters. Firstly, the low Cherenkov light yield and severe light attenuation of lead glass result in poor energy resolution. Lead fluoride crystals, which have less light attenuation, can be used instead, but they are much more expensive. Another disadvantage is the poor radiation resistance. While radiation-resistant types of lead glass can be used to improve this, they suffer from worse light attenuation. Additionally, due to the low light yield, the Cherenkov light being mainly in the UV range, and the detector being in a magnetic field, large-sized UV-sensitive SiPMs are required. These drawbacks present challenges for the usage of lead glass in this project.

One option is to use the ADRIANO2 [125] dual-readout calorimeter currently being developed by the REDTOP group. This design combines scintillation material and lead glass to capture both Cherenkov light and scintillation light signals. It employs longitudinal layering and readout, providing excellent energy resolution and additional capability for low-energy particle identification. This design addresses the shortcomings of using lead glass alone.

With the application of full silicon tracker of small pixel size, the momenta of charged particles are measured very precisely with a high event rate, and the sizes of all detectors scale down, which all depends on the size of inner tracker. It is a compact spectrometer with a large acceptance for the fixed-target experiment, and with competitive functions. The LGAD detector for time of flight measurement has a small time resolution and a very low material budget. The lead glass calorimeter is effective in reducing the neutron background, but its energy resolution is not so good. We also look for the new technologies of EM calorimeter which is capable to work in a high event rate environment. Therefore, with the current design of the spectrometer for Huizhou eta factory, we focus more on the charged decay channels of  $\eta$  meson. The radiation dosage for the spectrometer is simulated with both Geant4 [118–120] and FLUKA [126–128]. Under the circumstance of 100 MHz of inelastic scattering rate over a one-month data-taking period, the innermost LGAD is expected to experience a maximum 1 MeV neutron equivalent fluence of  $3 \times 10^{12} n_{\text{eq}}/\text{cm}^2$  and a maximum dose of 200 Gy. Meanwhile, the lead glass of EM calorimeter is expected to experience a maximum 1 MeV neutron equivalent fluence of  $5 \times 10^{11} n_{\text{eq}}/\text{cm}^2$  and a maximum dose of 100 Gy. Thus, these sub systems can survive several years before significant radiation damage occurs.

## 4 Some preliminary results of simulations

To see the physics impact and the feasibility of the experiment, we have performed some simulation studies of some golden channels for the Huizhou eta factory project. The simulation study is the first step for us to acquire the details regarding the resolutions, the efficiency of the signal channel, the background distribution, the precision of the planed measurement, and (or) the sensitivity to the new physics.

For the background events in p-A collisions, we use GiBUU event generator [121–124] to do the simulation. GiBUU is suitable for the proton-induced nuclear reactions from low energy to intermediate energy, with the final-state interactions well handled [121]. GiBUU event generator is based on the dynamical evolution of a colliding nucleus-nucleus system within the relativistic Boltzmann-Uehling-Uhlenbeck framework, which takes the hadronic potentials, the equation of state of nuclear matter, and the collision terms into account. In GiBUU, the low-energy collision is dominated by the resonance processes, while the high-energy collision is described with a string fragmentation model implemented in Pythia. For the  $\eta$  production,  $N^*(1720)$  in the process  $NN \rightarrow NR$  plays a dominant role [129]. Thus, GiBUU event generator covers perfectly the kinematical regions of HIAF and CiADS accelerator facilities.

In our simulation, the kinematic energy of the proton beam is 1.8 GeV, which is just below the  $\rho$  meson production threshold to lower the background. With the lithium target, we find that the number of neutrons is about one thousand times of the number of  $\eta$  mesons, and the number of  $\pi^0$  mesons is about 50 times of that of  $\eta$  mesons. The decay chains of  $\pi^0$  and  $\eta$  are further coded by us. For the signal event generations of the dark portal particles, we composed a simple event generator for the channels of interests. We also use another BUU generator [130] and the Urqmd package [131–133] to estimate the  $\eta$  production cross section. The  $\eta$  production probability is 0.76% in the inelastic collisions.

To quantify the detection efficiency and the resolutions, we have developed a detector simulation package ChnsRoot, which is based on the FairRoot framework [134, 135]. For now, we have the reliable fast simulation tool, which is based on the parametrizations validated by Geant4 simulations. The inner-most and outer-most radii of the silicon pixel tracker are 7.5 cm and 27.5 cm respectively. The magnetic field strength is 0.8 Tesla. The energy resolution of the calorimeter is  $\delta(E)/E = \sqrt{a^2 + b^2/(E/\text{GeV})}$  for the photon, with  $a = 0.028$  and  $b = 0.056$  estimated with Geant4. The neutron efficiency of the calorimeter as a function of the energy and the scattering angle is also studied with Geant4 in details. The calorimeter's responses to different types of particles are carefully studied, in order to have a realistic fast simulation of the spectrometer.

To understand the physics impact of the measurement, the statistic of the produced  $\eta$  samples is the most important input for the simulation. To be conservative on our experimental projections, in this simulation, we consider a prior experiment of only one-month running. Based on the evaluated luminosity and  $p$ -A cross section, the potential production rate of  $\eta$  can be above  $10^8 \text{ s}^{-1}$ , with the inelastic event rate around  $10^{10} \text{ s}^{-1}$ . The silicon pixel detector of high granularity is capable of working at a high event rate ( $> 100 \text{ MHz}$ ) without significant pile-ups of events. Nevertheless, considering the radiation hardness of the detector and the limit of current data acquisition (DAQ) system, we make a very conservative estimation of the event rate for Huizhou  $\eta$  factory experiment. The event rate of inelastic scattering is assumed to 100 MHz, and the  $\eta$  production rate is about 760 KHz. We also assume a conservative duty factor of the accelerator, which is 30%. With these settings, the number of  $\eta$  mesons produced is  $5.9 \times 10^{11}$  for the very first experiment of only one-month running time. Thus in the following simulations, we assume only  $5.9 \times 10^{11}$  eta mesons produced in the prior experiment.

The statistic of  $\eta$  meson samples can be increased magnitudes higher, since the experiment will run for years, the event rate can also be increased with the improvements of detector radiation hardness and speed of DAQ system, and the proton beam can be delivered to the high-energy terminal with a high duty factor.

### 4.1 Dark photon search

The decay channel  $\eta \rightarrow e^+e^-\gamma$  is of particular interests, as this channel is relevant for the search of the dark photon [34–37] and the light protophobic X17 boson [5–7] which decay into the electron-positron pair. At the same time, from the precise measurement of this channel, we can precisely extract the transition form factor of  $\eta$ , which is an important input for the theoretical calculation of muon anomalous moment  $(g-2)_\mu$ . The dark photon is the most popular dark portal particle which feebly connects the SM model sector with the possible hidden sector. Here we focus on the physics impact on the dark photon from the simulation data of Huizhou eta factory experiment.

Fig. 4 shows the kinematic distributions of the final-state particles of the channel  $e^+e^-\gamma$ , from the event

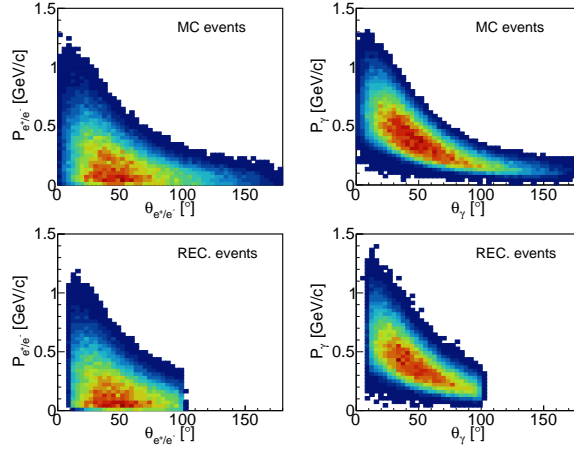


Figure 4: The momentum v.s. angle distributions of the final-state particles of  $\eta \rightarrow e^+e^-\gamma$  decay channel. The top pads show the kinematic distributions of the final states from the event generator, while the bottom pads show the the kinematic distributions of the reconstructed particles from the fast detector simulation. The designed spectrometer covers the main and a large kinematic region of the final-state particles.

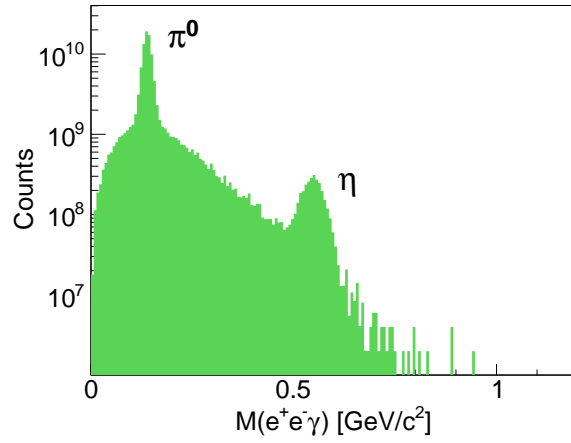


Figure 5: The invariant mass distribution of  $e^+e^-\gamma$  from the simulation data for one-month running of Huizhou  $\eta$  factory experiment.



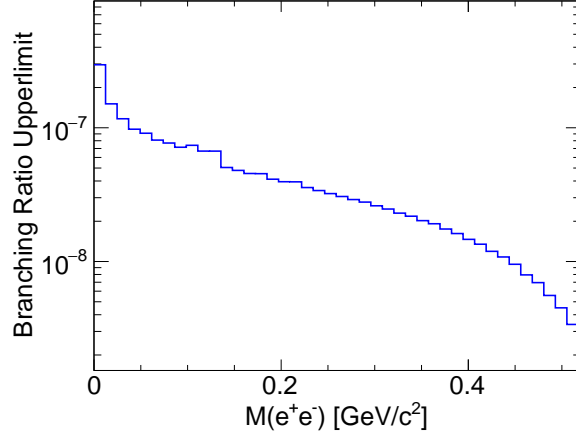


Figure 6: The estimated branching-ratio upperlimit of dark photon for just one-month running of Huizhou  $\eta$  factory experiment, under a conservative event rate of 100 MHz of inelastic reactions.

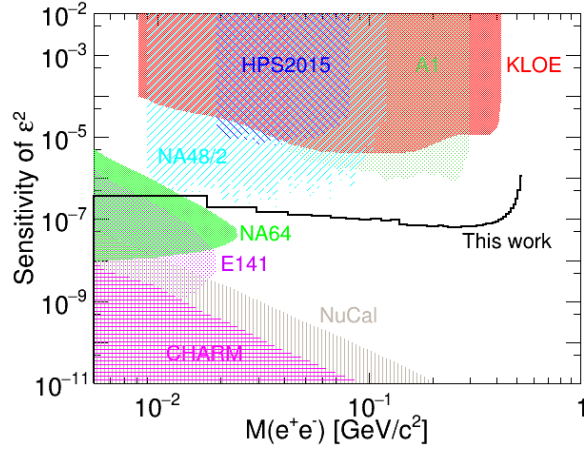


Figure 7: The estimated  $\varepsilon^2$  sensitivity of dark photon, for just one-month running of Huizhou  $\eta$  factory experiment, under a conservative event rate of 100 MHz of inelastic reactions. The shaded exclusion areas in the figure of previous experiments (HPS2015, A1@MAMI, KLOE, NA48/2, NA64, E141, NuCal and CHARM) are taken from Refs. [136–144].

generator and the particle reconstruction of the spectrometer simulation. One sees that the majority of the final electrons are of low momentum ( $< 0.5$  GeV/c) and go to a angle from  $10^\circ$  to  $100^\circ$ . The average energy of the final photon is about 0.4 GeV, and the photons are of the similar scattering angles of the electrons. The designed spectrometer just covers the most of the electrons and photons, the overall efficiency for the channel is estimated to be 60% with the simulation. For the low-energy electron, it can be effectively identified with the energy decomposition  $dE/dx$  measured by the silicon pixel tracker. And for the high-energy electron, it can be identified with the help of the calorimeter, as the pion initiates very few Cherenkov photons in the lead glass calorimeter.

The distribution of reconstructed invariant mass of  $e^+e^-\gamma$  is shown in Fig. 5. One sees clearly the peaks of  $\pi^0$  and  $\eta$  with just very low background underneath. Owing to the suppression of bremsstrahlung radiations in the proton scattering process, the electron and photon backgrounds are not significant. The  $\eta$  samples can be selected with a high purity by performing a cut on the invariant mass of  $e^+e^-\gamma$ . In this simulation study, the invariant mass is required to be in the range of  $[m_\eta - 3\sigma, m_\eta + 3\sigma]$ .

To estimate the sensitivity of the proposed experiment to the dark photon, we carefully studied the background distribution with the simulation. The background events are generated with GiBUU and with some decay chains added by us. In the simulation data, there is no bump in the invariant mass distribution of electron and position. We assume there is no dark photon in the simulation and the invariant mass distribution of  $e^+e^-$  is the pure background distribution. No observation of the dark photon means that the statistical significance of the dark photon peak is smaller than  $3\sigma$ . As a result, we get a formula for the branching-ratio (BR) upper limit of the dark photon channel, which is given by,

$$\text{BR}^{\text{up}} = \frac{3 \times \sqrt{N_{\text{bg}} \times \epsilon_{\text{bg}}}}{N_\eta \times \epsilon_{\text{sig}}}, \quad (1)$$

where  $N_{\text{bg}}$  is the number of background events,  $\epsilon_{\text{bg}}$  is efficiency for the background event,  $N_\eta$  is the total number of eta mesons produced in the experiment, and  $\epsilon_{\text{sig}}$  is the efficiency for the dark photon channel.  $N_{\text{bg}} \times \epsilon_{\text{bg}}$  is actually the number of background events survived after all the event selections. Based on the simulation of one-month experiment of Huizhou eta factory, the BR upper limit of dark photon in  $\eta$  decay is evaluated and shown in Fig. 6. The sensitivity of kinematic mixing parameter  $\epsilon^2$  is closely related to the upper limit of branching ratio, which is written as,

$$S(\epsilon^2) = \frac{\text{BR}^{\text{up}}}{2|F(m_A^2)|^2 \left(1 - \frac{m_A^2}{m_\eta^2}\right)^3}, \quad (2)$$

in which  $m_A$  and  $m_\eta$  are the masses of the dark photon and the  $\eta$  meson respectively, and  $F$  is the transition form factor of  $\eta$ . The final  $\epsilon^2$  sensitivity of one-month experiment to the dark photon is shown in Fig. 7. Our simulation indicates a significant sensitivity to  $\epsilon^2$ , below  $10^{-7}$ , which surpass the precisions of the previous experimental measurements (HPS2015 [136], A1@MAMI [137], KLOE [138], NA48/2 [139], NA64 [140], E141 [141], NuCal [142, 143] and CHARM [144]). The proposed experiment will be a valuable compliment to other dark photon searches. With years running of the experiment, the parameter space below the  $\eta$  mass will be almost ruled out combined with many other experiments worldwide [136, 137, 142–150].

## 4.2 Light dark higgs search

The light dark higgs [38–44] is another representative dark portal particle, which couples the hidden scalar field with the Higgs doublet. The dark higgs is thus weakly connected with the leptons and quarks via the Yukawa coupling. Therefore the dark higgs can be produced in the hadronic process and it can decays into lepton pairs and quark pairs. In a hadrophilic scalar model, the dark higgs mainly couples to the up quark, thus it dominantly decays into pions. At Huizhou eta factory, we could search for the dark higgs in the following channels:  $\eta \rightarrow \pi^0 h \rightarrow \pi^0 e^+e^-$  and  $\eta \rightarrow \pi^0 h \rightarrow \pi^0 \pi^+\pi^-$ . In these  $\eta$  rare decay channels, a bump in the invariant mass distribution of  $e^+e^-$  or  $\pi^+\pi^-$  is a clear signal of the possible dark scalar particle.

The distribution of reconstructed invariant mass of  $\pi^+\pi^-\pi^0$  is shown in Fig. 8. One sees clearly the peak of  $\eta$  meson with a low background underneath. In GiBUU simulation, the background from the direct multi-pion production is low compared to the  $\eta$  production, as the incident energy of proton is not large (1.8 GeV). The  $\eta$  samples from  $\pi^+\pi^-\pi^0$  can be selected with a high purity by performing a cut on the invariant mass of  $\pi^+\pi^-\pi^0$  in the range of  $[m_\eta - 3\sigma, m_\eta + 3\sigma]$ . The low background does not hinder much our explorations for the rare decays of  $\eta$  meson.

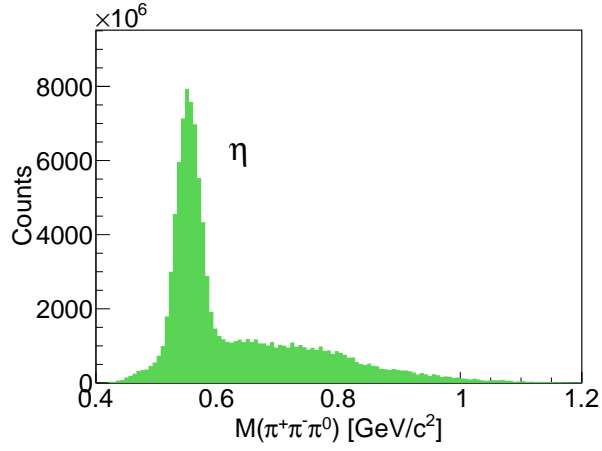


Figure 8: The invariant mass distribution of  $\pi^+\pi^-\pi^0$  from the simulation data for one-month running of Huizhou  $\eta$  factory experiment.

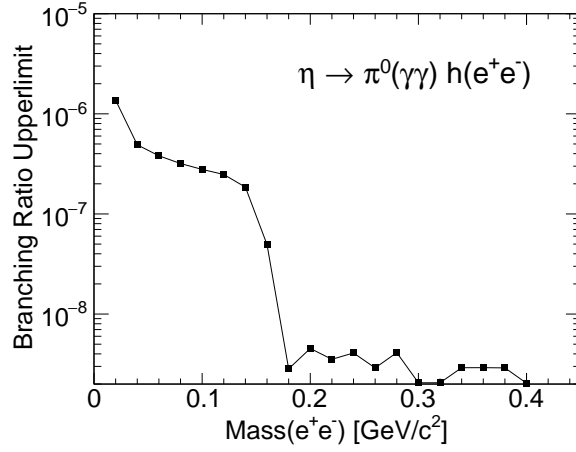


Figure 9: The estimated branching-ratio upperlimit of light dark higgs particle from  $\pi^0 e^+ e^-$  channel for just one-month running of Huizhou  $\eta$  factory experiment, under a conservative event rate of 100 MHz of inelastic reactions. The invariant mass of  $\pi^0 e^+ e^-$  is required to be in the  $\eta$  mass region.

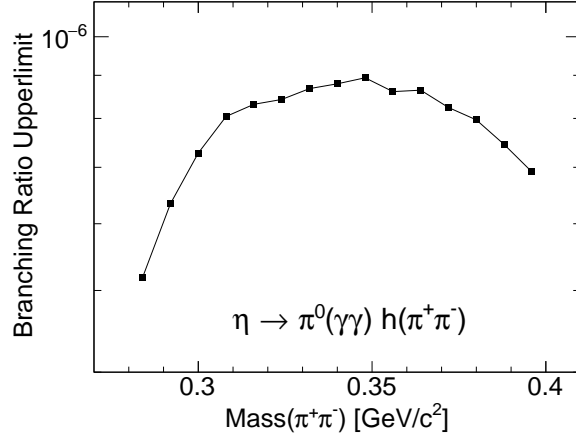


Figure 10: The estimated branching-ratio upperlimit of light dark higgs particle from  $\pi^0\pi^+\pi^-$  channel for just one-month running of Huizhou  $\eta$  factory experiment, under a conservative event rate of 100 MHz of inelastic reactions. The invariant mass of  $\pi^0\pi^+\pi^-$  is required to be in the  $\eta$  mass region.

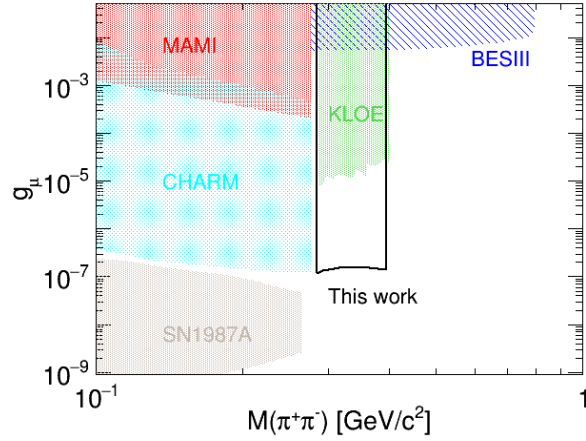


Figure 11: The estimated  $g_u$  sensitivity of light dark higgs particle in a hadrophilic scalar model [40, 41], for just one-month running of Huizhou  $\eta$  factory experiment, under a conservative event rate of 100 MHz of inelastic reactions. The previous experimental data for the shaded exclusion areas (BESIII, KLOE, MAMI, CHARM, and SN1987A) in the figure are taken from Refs. [40, 83, 151–154].

From the simulation, the efficiencies of  $\pi^0 e^+ e^-$  channel and  $\pi^0 \pi^+ \pi^-$  channel are all above 40% with the conceptual design of spectrometer. The resolutions for invariant masses of  $e^+ e^-$  and  $\pi^+ \pi^-$  are 2 MeV/c<sup>2</sup> and 1 MeV/c<sup>2</sup> respectively. In our studies, the bin width for the invariant mass is six times of the resolution. The background distributions without the dark higgs particle are simulated with the GiBUU event generator, and the total number of inelastic scattering events scales up to  $5.9 \times 10^{11}$ . Since there is no dark higgs observed in our simulation data, the upper limit of branching ratio of the dark higgs particle is given with the formula in Eq. (1). The BR upper limits of the light dark higgs particle in  $\pi^0 e^+ e^-$  and  $\pi^0 \pi^+ \pi^-$  channels are shown in Fig. 9 and Fig. 10 respectively, as a function of the mass of the dark higgs.

From Fig. 10, one sees that BR upper limit of dark higgs in  $\eta \rightarrow \pi^0 \pi^+ \pi^-$  channel is at the level of  $10^{-6}$  to  $10^{-7}$ , for one-month running of the experiment. From Fig. 9, one sees that the upper limit in  $\pi^0 e^+ e^-$  channel is obviously below  $10^{-8}$  in the most range of dark higgs mass. This is mainly due to the less electron background in  $p - A$  collisions, comparing to the strong pion background. One also finds that the upper limit in  $e^+ e^-$  channel falls down quickly, reaching a value below  $10^{-8}$  when the mass is above 0.14 GeV. This is because most of the  $e^+ e^-$  background comes from the  $\pi^0$  decay. Therefore the  $e^+ e^-$  channel has the advantage in searching the dark higgs of the mass heavier than the pion mass. With years running of the Huizhou eta factory experiment, we are confident that the accumulated data would provide the strong constraints of the possible dark higgs particle.

Under the hadrophilic scalar model [40, 41], the sensitivity to the parameter  $g_u$  (the coupling of dark scalar to the first-generation quark) is computed and shown in Fig. 11, compared with the constraints provided by the previous experimental data (BESIII [151], KLOE [83], MAMI [152], CHARM [153, 154] and SN1987A [40]). One finds that the  $g_u$  sensitivity from one-month running of the proposed Huizhou  $\eta$  factory will exceed the current experimental limits in the accessed mass range. The proposed super  $\eta$  factory will play an important role in searching the light dark scalar portal particles.

### 4.3 C and CP violation in $\eta \rightarrow \pi^+ \pi^- \pi^0$

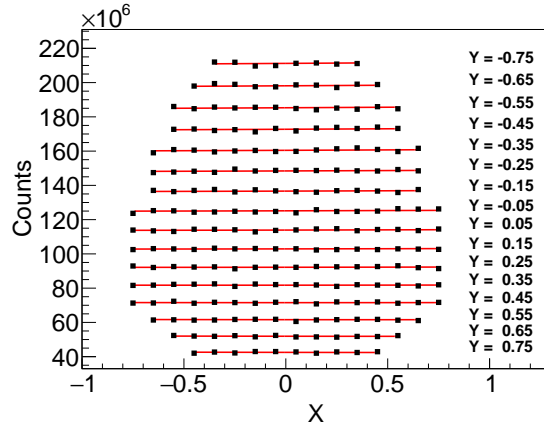


Figure 12: The event distributions of  $\eta \rightarrow \pi^+ \pi^- \pi^0$  decay channel (black squares) in different  $X$  and  $Y$  bins, for just one-month running of Huizhou  $\eta$  factory experiment, under a conservative event rate of 100 MHz of inelastic reactions. The Dalitz distribution of  $\eta \rightarrow \pi^+ \pi^- \pi^0$  is fitted with a simple model (the red lines). See the main text for more explanations.

The CP violation in the flavor-nondiagonal process due to the Cabibbo-Kobayashi-Maskawa (CKM) matrix phase is not enough to explain the matter-antimatter asymmetry in the universe. Therefore, searching for new sources and flavor-diagonal CP violation has been a hot topic in high-energy physics. The  $\pi^+ \pi^- \pi^0$  decay channel of  $\eta$  meson is of particular interests, since it provides a unique process to probe the flavor-diagonal C and CP violation beyond the SM. This type of CP violation is not constrained by the measurement of nucleon Electro-Dipole Moment (EDM), thus it lacks of the experimental study of high precision [33]. Owing to the interference between the C-conserving and C-violating amplitudes, the CP violation signal can be large. It is possible to find the small C and CP violation from a precise measurement of the mirror symmetry in the Dalitz decay plot of  $\pi^+ \pi^- \pi^0$  channel.

The direct observable of the charge asymmetry and CP violation is the mirror symmetry breaking in the Dalitz plot of  $\eta \rightarrow \pi^+\pi^-\pi^0$ , i.e. the asymmetry under the exchange of  $u$  and  $t$  ( $u \equiv (p_{\pi^+} + p_{\pi^0})^2$ ,  $t \equiv (p_{\pi^-} + p_{\pi^0})^2$ , and  $s \equiv (p_{\pi^+} + p_{\pi^-})^2$ ). The C and CP violation is reflected in the asymmetry of the decay events of  $u > t$  and  $u < t$ . Usually, the mirror asymmetry is vividly illustrated in the Dalitz plot of X and Y variables, which are defined as,

$$\begin{aligned} X &\equiv \sqrt{3} \frac{T_{\pi^+} - T_{\pi^-}}{Q_\eta} = \frac{\sqrt{3}}{2m_\eta Q_\eta} (u - t), \\ Y &\equiv \frac{3T_{\pi^0}}{Q_\eta} - 1 = \frac{3}{2m_\eta Q_\eta} [(m_\eta - m_{\pi^0})^2 - s] - 1, \end{aligned} \quad (3)$$

where  $Q_\eta = m_\eta - m_{\pi^+} - m_{\pi^-} - m_{\pi^0}$  and  $T_{\pi^i}$  are the total kinematic energy and the kinematic energy of  $\pi^i$  in the  $\eta$  rest frame. The distribution asymmetry across  $X = 0$  is a observable of the new type of CP violation. The Dalitz distribution of the decay probability can be conveniently parameterized as a polynomial expansion, which is written as,

$$\begin{aligned} N(X, Y) = N_0 &(1 + aY + bY^2 + cX + dX^2 + eXY \\ &+ fY^3 + gX^2Y + hXY^2 + lX^3 + \dots), \end{aligned} \quad (4)$$

in which  $a, b, c, \dots$  are free parameters. The nonzero value of the parameter  $c, e, h$ , or  $l$  is a strong indication of the flavor-diagonal C and CP violation.

The  $\pi^+\pi^-\pi^0$  channel is one of the major decay channels of  $\eta$  meson, and we can get a huge amount of the decay events from Huizhou eta factory experiment. From the simulation, the efficiency for the 3 pion channel is estimated to be approximate 45%. The event distributions in different X and Y bins are shown in Fig. 12, for one-month running of the experiment. The statistical error bars are too small to appear in the figure. We performed a model fit to the data with Eq. (4). The uncertainty of the parameter  $c$  is about  $5 \times 10^{-5}$ , which is two magnitudes smaller than the current analyses of COSY and KLOE-II data [77, 83]. With years running of the project, the C and CP violation can be tested at a splendid level of precision.

#### 4.4 Low-background $\eta$ data from exclusive channel $pd \rightarrow \eta \ ^3\text{He}$

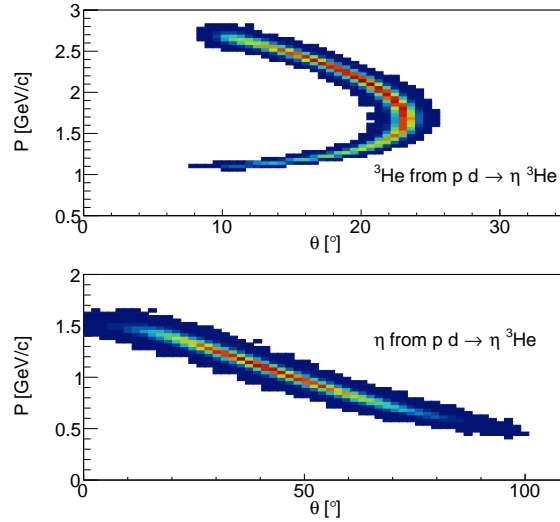


Figure 13: The kinematic distributions of the reconstructed  $^3\text{He}$  and  $\eta$  from a fast simulation of the spectrometer. The scattering angle and the momentum are highly correlated for the particles in the reaction  $pd \rightarrow \eta \ ^3\text{He}$ . The angular and momentum resolutions are small from the silicon pixel tracker.

We emphasis here that the low-background data of  $\eta$  mesons can be achieved at Huizhou eta factory via the  $^3\text{He}$  tagged events of the reaction  $pd \rightarrow \eta \ ^3\text{He}$ . In addition to the exclusivity of the measurement, the

momentum and angle of the final-state particle are highly correlated in the two-body-to-two-body scattering process. By tagging  ${}^3\text{He}$  and a cut of the momentum-angle correlation, the background is enormously reduced. The cross section of  $pd \rightarrow \eta \text{ } {}^3\text{He}$  reaction is not small [101, 155–159], which is  $0.4 \mu\text{b}$  near the production threshold measured by COSY-ANKE collaboration [157]. Note that the multiplicity of the final particles using deuterium target is much smaller than that using other nuclear targets. Therefore the event rate for  $pd \rightarrow \eta \text{ } {}^3\text{He}$  measurement can be set at a much higher rate, to increase the statistic of the low-background data.

Fig. 13 shows the two-dimensional kinematic distributions of  ${}^3\text{He}$  and  $\eta$  in the momentum vs. angle plane. One sees that the final  ${}^3\text{He}$  mainly goes to the region of scattering angle from  $15^\circ$  to  $25^\circ$ , while the  $\eta$  meson has the scattering angle mainly in the range from  $20^\circ$  to  $70^\circ$ . The conceptual design of the spectrometer is just suitable for tagging  ${}^3\text{He}$  and collecting the decay particles of  $\eta$  meson with a large acceptance. From Fig. 13, one sees that the momentum and angular resolutions of the silicon pixel tracker are excellent in picking up the exclusive events of  $pd \rightarrow \eta \text{ } {}^3\text{He}$ .

In short, with the high-intensity proton beam and the deuterium target, we could have a measurement of both high luminosity and high precision at Huizhou eta factory. This high-statistic and low-background data is precious and valuable in searching the new light particles, looking for the violations of CP and other discrete symmetries, measuring the transition form factor and  $u - d$  quark mass difference, and testing the low-energy effective theory of strong interaction. The systematic uncertainty from the background can be well controlled with the tagged  $\eta$  data of  $pd \rightarrow \eta \text{ } {}^3\text{He}$ .

## 5 Summary and outlook

A super  $\eta$  factory at Huizhou is proposed to pursue a variety of meaningful and challenging physical goals. The HIAF accelerator complex and the conceptual design of the spectrometer are briefly discussed. More than  $10^{13}$   $\eta$  mesons can be produced with 100% duty factor of the accelerator. The performance of the spectrometer is studied with Geant4 simulation, demonstrating satisfactory efficiency and resolution. The designed spectrometer is particularly adept at detecting charged particles and exhibits the required radiation hardness for high-luminosity experiments.

Through simulations, some key channels of Huizhou  $\eta$  factory experiment are investigated. The preliminary results from the fast simulation manifest that the Huizhou  $\eta$  factory will play a crucial role in searching for the predicted light dark portal particles and new sources of CP violation. The proposed experiment has the potential to significantly constrain the parameter space of the dark photon in the low-mass region together with other experiments. The sensitivity to the light dark scalar particle is estimated to be at an unprecedented level. The C and CP violation in channel  $\eta \rightarrow \pi^+\pi^-\pi^0$  can be measured by at least two magnitudes more precise, comparing to the up-to-date measurement worldwide. Judged with the simulation, the conceptual design of the spectrometer is capable for measuring the tagged  $\eta$  events of the reaction  $pd \rightarrow \eta \text{ } {}^3\text{He}$ . The tagging  ${}^3\text{He}$  method provides a measurement of both high statistic and low background, which is vital for the precision study of  $\eta$  physics.

Upon completing the planned accumulation of  $\eta$  decay samples, we could increase the beam energy and produce the  $\eta'$  mesons. The physical goals of high-precision studies of  $\eta'$  meson decays closely resemble to those of  $\eta$  meson. An advantage of studying  $\eta'$  decay is the ability to explore dark portal particles in a wider mass range, given that  $\eta'$  meson is heavier than  $\eta$  meson. With the same spectrometer, we can also carry out high-precision studies on  $\eta'$  and  $\phi$  meson decays, thereby boosting the discovery potential of the proposed Huizhou  $\eta$  factory project.

To further improve the discovery potential of the spectrometer, it is essential to enhance its capacity for detecting neutral particles. The current lead-glass EM calorimeter exhibits standard energy resolution; therefore exploring new calorimeter technologies with fast response time ( $< 100$  ps) and small energy resolution ( $< 3.5\%$  at 1 GeV) is imperative. With the rapid developments of silicon photomultiplier and electronics, dual-readout calorimetry collecting scintillation photons and Cherenkov photons could be a viable option for updating the EM calorimeter. The scintillation material improves the energy resolution significantly, while the Cherenkov light gives the sharp time resolution. With the dual readout calorimeter, the ability of particle identification also can be enhanced by comparing scintillation signal amplitude and Cherenkov signal amplitude. Future developments in silicon pixel detector and electronics will benefit the proposed Huizhou  $\eta$  factory project, enabling improvements in radiation hardness and resolutions that will elevate the event-rate limit for the planned high-luminosity experiments.

## Acknowledgments

This work was supported by the National Natural Science Foundation of China under the Grant NOs. 12222512 and 12005266, the Strategic Priority Research Program of Chinese Academy of Sciences under the Grant NO. XDB34030300.

## References

- [1] *Fundamental Physics at the Intensity Frontier*, 5 2012.
- [2] D. P. Aguillard et al. Measurement of the Positive Muon Anomalous Magnetic Moment to 0.20 ppm. *Phys. Rev. Lett.*, 131(16):161802, 2023.
- [3] B. Abi et al. Measurement of the Positive Muon Anomalous Magnetic Moment to 0.46 ppm. *Phys. Rev. Lett.*, 126(14):141801, 2021.
- [4] T. Albahri et al. Measurement of the anomalous precession frequency of the muon in the Fermilab Muon  $g - 2$  Experiment. *Phys. Rev. D*, 103(7):072002, 2021.
- [5] A. J. Krasznahorkay et al. Observation of Anomalous Internal Pair Creation in Be8 : A Possible Indication of a Light, Neutral Boson. *Phys. Rev. Lett.*, 116(4):042501, 2016.
- [6] Jonathan L. Feng, Bartosz Fornal, Iftah Galon, Susan Gardner, Jordan Smolinsky, Tim M. P. Tait, and Philip Tanedo. Protophobic Fifth-Force Interpretation of the Observed Anomaly in  $^8\text{Be}$  Nuclear Transitions. *Phys. Rev. Lett.*, 117(7):071803, 2016.
- [7] Jonathan L. Feng, Bartosz Fornal, Iftah Galon, Susan Gardner, Jordan Smolinsky, Tim M. P. Tait, and Philip Tanedo. Particle physics models for the 17 MeV anomaly in beryllium nuclear decays. *Phys. Rev. D*, 95(3):035017, 2017.
- [8] Roel Aaij et al. Test of lepton universality in beauty-quark decays. *Nature Phys.*, 18(3):277–282, 2022. [Addendum: *Nature Phys.* 19, (2023)].
- [9] Roel Aaij et al. Tests of lepton universality using  $B^0 \rightarrow K_S^0 \ell^+ \ell^-$  and  $B^+ \rightarrow K^{*+} \ell^+ \ell^-$  decays. *Phys. Rev. Lett.*, 128(19):191802, 2022.
- [10] Roel Aaij et al. Test of lepton universality with  $\Lambda_b^0 \rightarrow p K^- \ell^+ \ell^-$  decays. *JHEP*, 05:040, 2020.
- [11] Rodrigo Alonso, Benjamín Grinstein, and Jorge Martin Camalich. Lepton universality violation and lepton flavor conservation in  $B$ -meson decays. *JHEP*, 10:184, 2015.
- [12] Sonali Patnaik, Lopamudra Nayak, and Rajeev Singh. Assessing Lepton Flavor Universality Violations in Semileptonic Decays. 8 2023.
- [13] G. Ambrosi et al. Direct detection of a break in the teraelectronvolt cosmic-ray spectrum of electrons and positrons. *Nature*, 552:63–66, 2017.
- [14] Oscar Adriani et al. An anomalous positron abundance in cosmic rays with energies 1.5-100 GeV. *Nature*, 458:607–609, 2009.
- [15] J. Chang et al. An excess of cosmic ray electrons at energies of 300-800 GeV. *Nature*, 456:362–365, 2008.
- [16] F. Aharonian et al. The energy spectrum of cosmic-ray electrons at TeV energies. *Phys. Rev. Lett.*, 101:261104, 2008.
- [17] Pierre Jean et al. Early SPI / INTEGRAL measurements of 511 keV line emission from the 4th quadrant of the Galaxy. *Astron. Astrophys.*, 407:L55, 2003.
- [18] A. Arbey and F. Mahmoudi. Dark matter and the early Universe: a review. *Prog. Part. Nucl. Phys.*, 119:103865, 2021.



- [19] Eugene Oks. Brief review of recent advances in understanding dark matter and dark energy. *New Astron. Rev.*, 93:101632, 2021.
- [20] Gianfranco Bertone and Tim Tait, M. P. A new era in the search for dark matter. *Nature*, 562(7725):51–56, 2018.
- [21] Bing-Lin Young. A survey of dark matter and related topics in cosmology. *Front. Phys. (Beijing)*, 12(2):121201, 2017. [Erratum: *Front.Phys.(Beijing)* 12, 121202 (2017)].
- [22] Jonathan L. Feng. Dark Matter Candidates from Particle Physics and Methods of Detection. *Ann. Rev. Astron. Astrophys.*, 48:495–545, 2010.
- [23] Joshua Frieman, Michael Turner, and Dragan Huterer. Dark Energy and the Accelerating Universe. *Ann. Rev. Astron. Astrophys.*, 46:385–432, 2008.
- [24] Sunny Vagnozzi, Luca Visinelli, Philippe Brax, Anne-Christine Davis, and Jeremy Sakstein. Direct detection of dark energy: The XENON1T excess and future prospects. *Phys. Rev. D*, 104(6):063023, 2021.
- [25] Austin Joyce, Lucas Lombriser, and Fabian Schmidt. Dark Energy Versus Modified Gravity. *Ann. Rev. Nucl. Part. Sci.*, 66:95–122, 2016.
- [26] Miao Li, Xiao-Dong Li, Shuang Wang, and Yi Wang. Dark Energy: A Brief Review. *Front. Phys. (Beijing)*, 8:828–846, 2013.
- [27] Kenath Arun, S. B. Gudennavar, and C. Sivaram. Dark matter, dark energy, and alternate models: A review. *Adv. Space Res.*, 60:166–186, 2017.
- [28] Brian Batell, Maxim Pospelov, and Adam Ritz. Exploring Portals to a Hidden Sector Through Fixed Targets. *Phys. Rev. D*, 80:095024, 2009.
- [29] Gaia Lanfranchi, Maxim Pospelov, and Philip Schuster. The Search for Feebly Interacting Particles. *Ann. Rev. Nucl. Part. Sci.*, 71:279–313, 2021.
- [30] R. L. Workman et al. Review of Particle Physics. *PTEP*, 2022:083C01, 2022.
- [31] J. Elam et al. The REDTOP experiment: Rare  $\eta/\eta'$  Decays To Probe New Physics. 3 2022.
- [32] Liping Gan, Bastian Kubis, Emilie Passemar, and Sean Tulin. Precision tests of fundamental physics with  $\eta$  and  $\eta'$  mesons. *Phys. Rept.*, 945:1–105, 2022.
- [33] Susan Gardner and Jun Shi. Patterns of CP violation from mirror symmetry breaking in the  $\eta \rightarrow \pi^+ \pi^- \pi^0$  Dalitz plot. *Phys. Rev. D*, 101(11):115038, 2020.
- [34] Bob Holdom. Two U(1)’s and Epsilon Charge Shifts. *Phys. Lett. B*, 166:196–198, 1986.
- [35] Peter Galison and Aneesh Manohar. TWO Z’s OR NOT TWO Z’s? *Phys. Lett. B*, 136:279–283, 1984.
- [36] Pierre Fayet. Extra U(1)’s and New Forces. *Nucl. Phys. B*, 347:743–768, 1990.
- [37] Pierre Fayet. On the Search for a New Spin 1 Boson. *Nucl. Phys. B*, 187:184–204, 1981.
- [38] C. P. Burgess, Maxim Pospelov, and Tonnies ter Veldhuis. The Minimal model of nonbaryonic dark matter: A Singlet scalar. *Nucl. Phys. B*, 619:709–728, 2001.
- [39] Donal O’Connell, Michael J. Ramsey-Musolf, and Mark B. Wise. Minimal Extension of the Standard Model Scalar Sector. *Phys. Rev. D*, 75:037701, 2007.
- [40] Brian Batell, Ayres Freitas, Ahmed Ismail, and David Mckeen. Probing Light Dark Matter with a Hadrophilic Scalar Mediator. *Phys. Rev. D*, 100(9):095020, 2019.
- [41] Brian Batell, Ayres Freitas, Ahmed Ismail, and David Mckeen. Flavor-specific scalar mediators. *Phys. Rev. D*, 98(5):055026, 2018.

- [42] Brian Patt and Frank Wilczek. Higgs-field portal into hidden sectors. 5 2006.
- [43] Vanda Silveira and A. Zee. SCALAR PHANTOMS. *Phys. Lett. B*, 161:136–140, 1985.
- [44] Maxim Pospelov, Adam Ritz, and Mikhail B. Voloshin. Secluded WIMP Dark Matter. *Phys. Lett. B*, 662:53–61, 2008.
- [45] Howard Georgi, David B. Kaplan, and Lisa Randall. Manifesting the Invisible Axion at Low-energies. *Phys. Lett. B*, 169:73–78, 1986.
- [46] Martin Bauer, Matthias Neubert, and Andrea Thamm. Collider Probes of Axion-Like Particles. *JHEP*, 12:044, 2017.
- [47] Daniel Aloni, Yotam Soreq, and Mike Williams. Coupling QCD-Scale Axionlike Particles to Gluons. *Phys. Rev. Lett.*, 123(3):031803, 2019.
- [48] Giacomo Landini and Enrico Meggiolaro. Study of the interactions of the axion with mesons and photons using a chiral effective Lagrangian model. *Eur. Phys. J. C*, 80(4):302, 2020.
- [49] Fatih Ertas and Felix Kahlhoefer. On the interplay between astrophysical and laboratory probes of MeV-scale axion-like particles. *JHEP*, 07:050, 2020.
- [50] Dmitry Gorbunov and Mikhail Shaposhnikov. How to find neutral leptons of the  $\nu$ MSM? *JHEP*, 10:015, 2007. [Erratum: *JHEP* 11, 101 (2013)].
- [51] Anupama Atre, Tao Han, Silvia Pascoli, and Bin Zhang. The Search for Heavy Majorana Neutrinos. *JHEP*, 05:030, 2009.
- [52] S. N. Gninenko. The MiniBooNE anomaly and heavy neutrino decay. *Phys. Rev. Lett.*, 103:241802, 2009.
- [53] Steven Weinberg. Phenomenological Lagrangians. *Physica A*, 96(1-2):327–340, 1979.
- [54] J. Gasser and H. Leutwyler. Chiral Perturbation Theory to One Loop. *Annals Phys.*, 158:142, 1984.
- [55] J. Gasser and H. Leutwyler. Chiral Perturbation Theory: Expansions in the Mass of the Strange Quark. *Nucl. Phys. B*, 250:465–516, 1985.
- [56] G. Ecker. Chiral perturbation theory. *Prog. Part. Nucl. Phys.*, 35:1–80, 1995.
- [57] A. Pich. Chiral perturbation theory. *Rept. Prog. Phys.*, 58:563–610, 1995.
- [58] Veronique Bernard and Ulf-G. Meissner. Chiral perturbation theory. *Ann. Rev. Nucl. Part. Sci.*, 57:33–60, 2007.
- [59] P. Aguilar-Bartolome et al. New determination of the  $\eta$  transition form factor in the Dalitz decay  $\eta \rightarrow e^+e^-\gamma$  with the Crystal Ball/TAPS detectors at the Mainz Microtron. *Phys. Rev. C*, 89(4):044608, 2014.
- [60] P. Adlarson et al. Measurement of the  $\omega \rightarrow \pi^0 e^+e^-$  and  $\eta \rightarrow e^+e^-\gamma$  Dalitz decays with the A2 setup at MAMI. *Phys. Rev. C*, 95(3):035208, 2017.
- [61] D. Pszczel and J. Stepaniak. Dielectron pairs from  $\eta$  meson decays at WASA detector. *EPJ Web Conf.*, 199:02011, 2019.
- [62] F. Ambrosino et al. Observation of the rare  $\eta \rightarrow e^+e^-e^+e^-$  decay with the KLOE experiment. *Phys. Lett. B*, 702:324–328, 2011.
- [63] M. Berlowski et al. Measurement of eta meson decays into lepton-antilepton pairs. *Phys. Rev. D*, 77:032004, 2008.
- [64] M. Ablikim et al. Observation of the Dalitz Decay  $\eta' \rightarrow \gamma e^+e^-$ . *Phys. Rev. D*, 92(1):012001, 2015.
- [65] R. Escribano, P. Masjuan, and P. Sanchez-Puertas. The  $\eta$  transition form factor from space- and time-like experimental data. *Eur. Phys. J. C*, 75(9):414, 2015.

- [66] Murray Gell-Mann, R. J. Oakes, and B. Renner. Behavior of current divergences under  $SU(3) \times SU(3)$ . *Phys. Rev.*, 175:2195–2199, 1968.
- [67] Steven Weinberg. The Problem of Mass. *Trans. New York Acad. Sci.*, 38:185–201, 1977.
- [68] Roger F. Dashen. Chiral  $SU(3) \times SU(3)$  as a symmetry of the strong interactions. *Phys. Rev.*, 183:1245–1260, 1969.
- [69] J. Gasser and H. Leutwyler.  $\eta \rightarrow 3\pi$  to One Loop. *Nucl. Phys. B*, 250:539–560, 1985.
- [70] David B. Kaplan and Aneesh V. Manohar. Current Mass Ratios of the Light Quarks. *Phys. Rev. Lett.*, 56:2004, 1986.
- [71] H. Leutwyler. The Ratios of the light quark masses. *Phys. Lett. B*, 378:313–318, 1996.
- [72] J. Wess and B. Zumino. Consequences of anomalous Ward identities. *Phys. Lett. B*, 37:95–97, 1971.
- [73] Edward Witten. Global Aspects of Current Algebra. *Nucl. Phys. B*, 223:422–432, 1983.
- [74] A. M. Bernstein and Barry R. Holstein. Neutral Pion Lifetime Measurements and the QCD Chiral Anomaly. *Rev. Mod. Phys.*, 85:49, 2013.
- [75] M. Jetter.  $\eta \rightarrow \pi^0 \gamma \gamma$  to  $O(p^6)$  in chiral perturbation theory. *Nucl. Phys. B*, 459:283–310, 1996.
- [76] P. Adlarson et al. Search for  $C$  violation in the decay  $\eta \rightarrow \pi^0 + e^+ + e^-$  with WASA-at-COSY. *Phys. Lett. B*, 784:378–384, 2018.
- [77] P. Adlarson et al. Measurement of the  $\eta \rightarrow \pi^+ \pi^- \pi^0$  Dalitz plot distribution. *Phys. Rev. C*, 90(4):045207, 2014.
- [78] Nils Hüsken, Kay Demmich, and Alfons Khoukaz.  $\eta$  meson physics with WASA-at-COSY. *EPJ Web Conf.*, 199:01006, 2019.
- [79] Roel Aaij et al. Production of  $\eta$  and  $\eta'$  mesons in pp and pPb collisions. *Phys. Rev. C*, 109(2):024907, 2024.
- [80] Roel Aaij et al. Search for the  $CP$ -violating strong decays  $\eta \rightarrow \pi^+ \pi^-$  and  $\eta'(958) \rightarrow \pi^+ \pi^-$ . *Phys. Lett. B*, 764:233–240, 2017.
- [81] Wojciech Krzemien and Elena Pérez del Río. The KLOE-2 experiment: Overview of recent results. *Int. J. Mod. Phys. A*, 34(25):1930012, 2019.
- [82] D. Babusci et al. Upper limit on the  $\eta \rightarrow \pi^+ \pi^-$  branching fraction with the KLOE experiment. *JHEP*, 10:047, 2020.
- [83] A. Anastasi et al. Precision measurement of the  $\eta \rightarrow \pi^+ \pi^- \pi^0$  Dalitz plot distribution with the KLOE detector. *JHEP*, 05:019, 2016.
- [84] F. Ambrosino et al. Measurement of the branching ratio and search for a CP violating asymmetry in the  $\eta \rightarrow \pi^+ \pi^- e^+ e^- (\gamma)$  decay at KLOE. *Phys. Lett. B*, 675:283–288, 2009.
- [85] M. Ablikim et al. Measurement of the absolute branching fractions of  $J/\psi \rightarrow \gamma \eta$  and  $\eta$  decay modes. *Phys. Rev. D*, 104(9):092004, 2021.
- [86] M. Ablikim et al. Measurement of the Matrix Elements for the Decays  $\eta \rightarrow \pi^+ \pi^- \pi^0$  and  $\eta/\eta' \rightarrow \pi^0 \pi^0 \pi^0$ . *Phys. Rev. D*, 92:012014, 2015.
- [87] Medina Ablikim et al. Evidence for the Cusp Effect in  $\eta'$  Decays into  $\eta \pi^0 \pi^0$ . *Phys. Rev. Lett.*, 130(8):081901, 2023.
- [88] Medina Ablikim et al. Precision Measurement of the Branching Fractions of  $\eta'$  Decays. *Phys. Rev. Lett.*, 122(14):142002, 2019.

- [89] M. Ablikim et al. Precision Study of  $\eta' \rightarrow \gamma\pi^+\pi^-$  Decay Dynamics. *Phys. Rev. Lett.*, 120(24):242003, 2018.
- [90] V. L. Kashevarov et al. Study of  $\eta$  and  $\eta'$  Photoproduction at MAMI. *Phys. Rev. Lett.*, 118(21):212001, 2017.
- [91] E. F. McNicoll et al. Study of the  $\gamma p \rightarrow \eta p$  reaction with the Crystal Ball detector at the Mainz Microtron(MAMI-C). *Phys. Rev. C*, 82:035208, 2010. [Erratum: *Phys.Rev.C* 84, 029901 (2011)].
- [92] Liping Gan et al. Update to the jef proposal (pr12-14-004). [https://www.jlab.org/exp\\_prog/proposals/17/C12-14-004.pdf](https://www.jlab.org/exp_prog/proposals/17/C12-14-004.pdf). Accessed June 18, 2024.
- [93] H. Primakoff. Photoproduction of neutral mesons in nuclear electric fields and the mean life of the neutral meson. *Phys. Rev.*, 81:899, 1951.
- [94] I. Larin et al. A New Measurement of the  $\pi^0$  Radiative Decay Width. *Phys. Rev. Lett.*, 106:162303, 2011.
- [95] I. Larin et al. Precision measurement of the neutral pion lifetime. *Science*, 368(6490):506–509, 2020.
- [96] S. Adhikari et al. The GLUEX beamline and detector. *Nucl. Instrum. Meth. A*, 987:164807, 2021.
- [97] A. Asaturyan et al. Electromagnetic calorimeters based on scintillating lead tungstate crystals for experiments at Jefferson Lab. *Nucl. Instrum. Meth. A*, 1013:165683, 2021.
- [98] J. C. Yang et al. High Intensity heavy ion Accelerator Facility (HIAF) in China. *Nucl. Instrum. Meth. B*, 317:263–265, 2013.
- [99] Jiancheng Yang, Daqing Gao, Yuan He, Lijun Mao, Guodong Shen, Lina Sheng, Liangting Sun, Zhe Xu, Yaqing Yang, and Youjin Yuan. Status of the HIAF Accelerator Facility in China. In *27th Russian Particle Accelerator Conference*, 10 2021.
- [100] Xiaohong Zhou and Jiancheng Yang. Status of the high-intensity heavy-ion accelerator facility in China. *AAPPS Bull.*, 32(1):35, 2022.
- [101] Colin Wilkin. The legacy of the experimental hadron physics programme at COSY. *Eur. Phys. J. A*, 53(6):114, 2017.
- [102] P. Moskal et al. Experimental study of pp eta dynamics in the pp  $\rightarrow$  pp eta reaction. *Phys. Rev. C*, 69:025203, 2004.
- [103] H. Petren et al. eta-meson production in proton-proton collisions at excess energies of 40 and 72 MeV. *Phys. Rev. C*, 82:055206, 2010.
- [104] H. Calen et al. Measurement of the quasifree p + n  $\rightarrow$  p + n + eta reaction near threshold. *Phys. Rev. C*, 58:2667–2670, 1998.
- [105] Y. He et al. Accelerator driven system - a solution to multiple problems of society. In *Proc. IPAC'23*, number 14 in IPAC'23 - 14th International Particle Accelerator Conference, pages 5205–5209. JACoW Publishing, Geneva, Switzerland, 05 2023.
- [106] Z.J. Wang et al. The Status of CiADS Superconducting LINAC. In *Proc. 10th International Particle Accelerator Conference (IPAC'19), Melbourne, Australia, 19-24 May 2019*, number 10 in International Particle Accelerator Conference, pages 994–997, Geneva, Switzerland, Jun. 2019. JACoW Publishing. <https://doi.org/10.18429/JACoW-IPAC2019-MOPTS059>.
- [107] S.H. Liu, W.L. Chen, W.P. Dou, Y. He, H. Jia, Y.S. Qin, Z.J. Wang, and H.W. Zhao. Commissioning of China ADS Demo Linac and Baseline Design of CiADS Project. In *Proc. HIAT'18*, number 14 in International Conference on Heavy Ion Accelerator Technology, pages 112–116. JACoW Publishing, Geneva, Switzerland, nov 2019. <https://doi.org/10.18429/JACoW-HIAT2018-WEYAA01>.
- [108] Shuhui Liu et al. Physics design of the superconducting section of the CiADS linac. *Int. J. Mod. Phys. A*, 34(29):1950178, 2019.

- [109] Zhi-Jun Wang et al. Beam physics design of a superconducting linac. *Phys. Rev. Accel. Beams*, 27(1):010101, 2024.
- [110] Han-Jie Cai et al. Towards a high-intensity muon source. *Phys. Rev. Accel. Beams*, 27(2):023403, 2024.
- [111] Rui He et al. Advances in nuclear detection and readout techniques. *Nucl. Sci. Tech.*, 34(12):205, 2023.
- [112] J.A. Appel, M.H. Bourquin, I. Gaines, D.C. Hom, L.M. Lederman, H.P. Paar, J.-P. Repellin, D.H. Saxon, H.D. Snyder, J.M. Weiss, J.K. Yoh, B.C. Brown, C.N. Brown, J.-M. Gaillard, J.R. Sauer, and T. Yamanouchi. Performance of a lead-glass electromagnetic shower detector at fermilab. *Nuclear Instruments and Methods*, 127(4):495–505, 1975.
- [113] Weiping Ren et al. Topmetal-M: a novel pixel sensor for compact tracking applications. 1 2022.
- [114] Haibo Yang et al. Hi’Beam-S: A Monolithic Silicon Pixel Sensor-Based Prototype Particle Tracking System for HIAF. *IEEE Trans. Nucl. Sci.*, 68(12):2794–2800, 2021.
- [115] Haibo Yang et al. Heavy-ion beam test of a monolithic silicon pixel sensor with a new 130 nm High-Resistivity CMOS process. *Nucl. Instrum. Meth. A*, 1039:167049, 2022.
- [116] Ping Yang et al. Design of Nupix-A1, a Monolithic Active Pixel Sensor for heavy-ion physics. *Nucl. Instrum. Meth. A*, 1039:167019, 2022.
- [117] J. Huang et al. Design of Nupix-A2, a Monolithic Active Pixel Sensor for heavy-ion physics. *JINST*, 18(11):C11014, 2023.
- [118] S. Agostinelli et al. GEANT4—a simulation toolkit. *Nucl. Instrum. Meth. A*, 506:250–303, 2003.
- [119] John Allison et al. Geant4 developments and applications. *IEEE Trans. Nucl. Sci.*, 53:270, 2006.
- [120] J. Allison et al. Recent developments in Geant4. *Nucl. Instrum. Meth. A*, 835:186–225, 2016.
- [121] O. Buss, T. Gaitanos, K. Gallmeister, H. van Hees, M. Kaskulov, O. Lalakulich, A. B. Larionov, T. Leitner, J. Weil, and U. Mosel. Transport-theoretical Description of Nuclear Reactions. *Phys. Rept.*, 512:1–124, 2012.
- [122] Giessen boltzmann-uehling-uhlenbeck project (gibuu). <https://gibuu.hepforge.org/>. Accessed June 18, 2024.
- [123] T. Gaitanos, H. Lenske, and U. Mosel. Fragment formation in proton induced reactions within a BUU transport model. *Phys. Lett. B*, 663:197–201, 2008.
- [124] Janus Weil, Hendrik van Hees, and Ulrich Mosel. Dilepton production in proton-induced reactions at SIS energies with the GiBUU transport model. *Eur. Phys. J. A*, 48:111, 2012. [Erratum: *Eur.Phys.J.A* 48, 150 (2012)].
- [125] Corrado Gatto, Gerald Blazey, Alexandre Dychkant, Jeffrey Elam, Michael Figora, Todd Fletcher, Kithisya Francis, Ao Liu, Sergey Los, Cole Mahieu, Anil Mane, Juan Marquez, Michael Murray, Erik Ramberg, Christophe Royon, Michael Syphers, Robert Young, and Vishnu Zutshi. Preliminary results from adriano2 test beams. *Instruments*, 6:49, 09 2022.
- [126] Giuseppe Battistoni et al. Overview of the FLUKA code. *Annals Nucl. Energy*, 82:10–18, 2015.
- [127] Fluka. <https://fluka.cern/>. Accessed June 18, 2024.
- [128] Fluka. <http://www.fluka.org/fluka.php>. Accessed June 18, 2024.
- [129] Qi-Fang Lü and De-Min Li. Near-threshold  $\eta$  production in pp collisions. *Chin. Phys. C*, 39(11):113104, 2015.
- [130] B. Li, A. T. Sustich, B. Zhang, and C. M. Ko. Studies of superdense hadronic matter in a relativistic transport model. *Int. J. Mod. Phys. E*, 10:267–352, 2001.

- [131] S. A. Bass et al. Microscopic models for ultrarelativistic heavy ion collisions. *Prog. Part. Nucl. Phys.*, 41:255–369, 1998.
- [132] M. Bleicher et al. Relativistic hadron hadron collisions in the ultrarelativistic quantum molecular dynamics model. *J. Phys. G*, 25:1859–1896, 1999.
- [133] Marcus Bleicher. Ultrarelativistic quantum molecular dynamics (urqmd). <https://itp.uni-frankfurt.de/~bleicher/index.html?content=urqmd>. Accessed June 18, 2024.
- [134] M. Al-Turany, D. Bertini, R. Karabowicz, D. Kresan, P. Malzacher, T. Stockmanns, and F. Uhlig. The FairRoot framework. *J. Phys. Conf. Ser.*, 396:022001, 2012.
- [135] Fairroot. <https://fairroot.gsi.de/>. Accessed June 18, 2024.
- [136] P. H. Adrian et al. Search for a dark photon in electroproduced  $e^+e^-$  pairs with the Heavy Photon Search experiment at JLab. *Phys. Rev. D*, 98(9):091101, 2018.
- [137] H. Merkel et al. Search for Light Gauge Bosons of the Dark Sector at the Mainz Microtron. *Phys. Rev. Lett.*, 106:251802, 2011.
- [138] Simona Giovannella et al. U boson searches at KLOE. *J. Phys. Conf. Ser.*, 335:012067, 2011.
- [139] J. R. Batley et al. Search for the dark photon in  $\pi^0$  decays. *Phys. Lett. B*, 746:178–185, 2015.
- [140] Sergei Gninenko. Addendum to the NA64 Proposal: Search for the  $A' \rightarrow \text{invisible}$  and  $X \rightarrow e^+e^-$  decays in 2021. Technical report, CERN, Geneva, 2018.
- [141] E. M. Riordan et al. A Search for Short Lived Axions in an Electron Beam Dump Experiment. *Phys. Rev. Lett.*, 59:755, 1987.
- [142] Johannes Blumlein and Jurgen Brunner. New Exclusion Limits for Dark Gauge Forces from Beam-Dump Data. *Phys. Lett. B*, 701:155–159, 2011.
- [143] Johannes Blümlein and Jürgen Brunner. New Exclusion Limits on Dark Gauge Forces from Proton Bremsstrahlung in Beam-Dump Data. *Phys. Lett. B*, 731:320–326, 2014.
- [144] S. N. Gninenko. Constraints on sub-GeV hidden sector gauge bosons from a search for heavy neutrino decays. *Phys. Lett. B*, 713:244–248, 2012.
- [145] P. H. Adrian et al. Searching for prompt and long-lived dark photons in electroproduced  $e^+e^-$  pairs with the heavy photon search experiment at JLab. *Phys. Rev. D*, 108(1):012015, 2023.
- [146] S. Abrahamyan et al. Search for a New Gauge Boson in Electron-Nucleus Fixed-Target Scattering by the APEX Experiment. *Phys. Rev. Lett.*, 107:191804, 2011.
- [147] James D. Bjorken, Rouven Essig, Philip Schuster, and Natalia Toro. New Fixed-Target Experiments to Search for Dark Gauge Forces. *Phys. Rev. D*, 80:075018, 2009.
- [148] L. Marsicano, M. Battaglieri, M. Bondi', C. D. R. Carvajal, A. Celentano, M. De Napoli, R. De Vita, E. Nardi, M. Raggi, and P. Valente. Dark photon production through positron annihilation in beam-dump experiments. *Phys. Rev. D*, 98(1):015031, 2018.
- [149] Brian Batell, Rouven Essig, and Ze'ev Surujon. Strong Constraints on Sub-GeV Dark Sectors from SLAC Beam Dump E137. *Phys. Rev. Lett.*, 113(17):171802, 2014.
- [150] J. D. Bjorken, S. Ecklund, W. R. Nelson, A. Abashian, C. Church, B. Lu, L. W. Mo, T. A. Nunamaker, and P. Rassmann. Search for Neutral Metastable Penetrating Particles Produced in the SLAC Beam Dump. *Phys. Rev. D*, 38:3375, 1988.
- [151] Medina Ablikim et al. Amplitude Analysis of the Decays  $\eta' \rightarrow \pi^+\pi^-\pi^0$  and  $\eta' \rightarrow \pi^0\pi^0\pi^0$ . *Phys. Rev. Lett.*, 118(1):012001, 2017.
- [152] B. M. K. Nefkens et al. New measurement of the rare decay  $\eta \rightarrow \pi^0\gamma\gamma$  with the Crystal Ball/TAPS detectors at the Mainz Microtron. *Phys. Rev. C*, 90(2):025206, 2014.

- [153] F. Bergsma et al. Search for Axion Like Particle Production in 400-GeV Proton - Copper Interactions. *Phys. Lett. B*, 157:458–462, 1985.
- [154] Yu-Sheng Liu, Ian C. Cloët, and Gerald A. Miller. Eta Decay and Muonic Puzzles. *Nucl. Phys.*, B:114638, 2019.
- [155] R. Bilger et al. Measurement of the  $p\,d \rightarrow \text{He-3}\,\eta$  cross-section between 930-MeV and 1100-MeV. *Phys. Rev. C*, 65:044608, 2002.
- [156] J. Smyski et al. Measurement of the  $dp \rightarrow \text{He-3}\,\eta$  reaction near threshold. *Phys. Lett. B*, 649:258–262, 2007.
- [157] T. Mersmann et al. Precision study of the  $\eta$  He-3 system using the  $dp \rightarrow \text{He-3}\,\eta$  reaction. *Phys. Rev. Lett.*, 98:242301, 2007.
- [158] T. Rausmann et al. Precision study of the  $dp \rightarrow \text{He-3}\,\eta$  reaction for excess energies between 20-MeV and 60-MeV. *Phys. Rev. C*, 80:017001, 2009.
- [159] P. Adlarson et al. Cross section ratio and angular distributions of the reaction  $p + d \rightarrow {}^3\text{He} + \eta$  at 48.8 MeV and 59.8 MeV excess energy. *Eur. Phys. J. A*, 50:100, 2014.